

Generation of dc spin current in a narrow channel with Rashba and Dresselhaus spin-orbit interactions

Chi-Shung Tang, Wen-Hsuan Kuan, Wen Xu, and Yia-Chung Chang

Citation: *Journal of Vacuum Science & Technology B* **26**, 1624 (2008); doi: 10.1116/1.2908440

View online: <http://dx.doi.org/10.1116/1.2908440>

View Table of Contents: <http://scitation.aip.org/content/avs/journal/jvstb/26/4?ver=pdfcov>

Published by the AVS: Science & Technology of Materials, Interfaces, and Processing

Articles you may be interested in

[Separation of Rashba and Dresselhaus spin-orbit interactions using crystal direction dependent transport measurements](#)

Appl. Phys. Lett. **103**, 252407 (2013); 10.1063/1.4855495

[Interplay of magnetic field and geometry in magneto-transport of mesoscopic loops with Rashba and Dresselhaus spin-orbit interactions](#)

J. Appl. Phys. **112**, 024321 (2012); 10.1063/1.4739485

[Determination of Rashba and Dresselhaus spin-orbit fields](#)


J. Appl. Phys. **110**, 064306 (2011); 10.1063/1.3632060

[Anisotropic magnetoplasmon spectrum of two-dimensional electron gas systems with the Rashba and Dresselhaus spin-orbit interactions](#)




J. Appl. Phys. **109**, 093306 (2011); 10.1063/1.3583651

[Pure spin current in a three-terminal spin device in the presence of Rashba spin-orbit interaction](#)

Appl. Phys. Lett. **91**, 092128 (2007); 10.1063/1.2777149



Instruments for Advanced Science

<p>Contact Hiden Analytical for further details: W www.HidenAnalytical.com E info@hiden.co.uk CLICK TO VIEW our product catalogue</p>	 <p>Gas Analysis</p> <ul style="list-style-type: none"> › dynamic measurement of reaction gas streams › catalysis and thermal analysis › molecular beam studies › dissolved species probes › fermentation, environmental and ecological studies 	 <p>Surface Science</p> <ul style="list-style-type: none"> › UHV TPD › SIMS › end point detection in ion beam etch › elemental imaging - surface mapping 	 <p>Plasma Diagnostics</p> <ul style="list-style-type: none"> › plasma source characterization › etch and deposition process reaction › kinetic studies › analysis of neutral and radical species 	 <p>Vacuum Analysis</p> <ul style="list-style-type: none"> › partial pressure measurement and control of process gases › reactive sputter process control › vacuum diagnostics › vacuum coating process monitoring
---	--	--	--	--

Generation of dc spin current in a narrow channel with Rashba and Dresselhaus spin-orbit interactions

Chi-Shung Tang^{a)}

Micro- and Nanotechnology Division, Department of Mechanical Engineering, National United University, Miaoli 36003, Taiwan

Wen-Hsuan Kuan^{b)}

Physics Division, National Center for Theoretical Sciences, Hsinchu 30013, Taiwan

Wen Xu^{c)}

Department of Theoretical Physics, Research School of Physical Sciences and Engineering, Australian National University, Canberra ACT0200, Australia

Yia-Chung Chang^{d)}

Research Center for Applied Sciences, Academia Sinica, Taipei 11529, Taiwan

(Received 30 October 2007; accepted 17 March 2008; published 15 August 2008)

The authors consider a finite range ac-biased front gate acting on a quantum channel with Rashba and Dresselhaus spin-orbit interaction effects. The ac-biased gate, giving rise to a dynamical Rashba coupling, causes spin-resolved coherent resonant inelastic scattering. A pure dc spin current is subsequently generated without accompanying charge current. In the presence of Dresselhaus effect, the dc spin current is suppressed in the regime but is assisted in the high kinetic energy regime.

© 2008 American Vacuum Society. [DOI: 10.1116/1.2908440]

Manipulation of electron spins is achievable with external active control, which is a central requirement of spintronic devices. Of fundamental interest and practical application is the spin current in the emerging field of spintronics.¹ One of the key issues is how to generate spin current in spintronic devices. The standard way is to inject spin polarized current from a ferromagnetic electrode.² However, its efficiency is usually limited by the poor quality of the interface, and it is accompanied by the charge current. Narrow gap semiconductor heterostructures offer an efficient control of spins through intrinsic spin-orbit interaction (SOI). Several approaches utilizing spin Hall effects,^{3–8} magnetic fields,^{9–12} ferromagnetic materials,^{13,14} or optical excitations^{15–17} were proposed.

The success of dc front-gate control for the measurement¹⁸ of Rashba coupling strength¹⁹ inspired proposals for spin current generation by nonmagnetic means.^{20–24} These proposals include adiabatic quantum pumping in a quantum dot with static SOI (Ref. 20) interfaced with a time-dependent barrier and a spatially separated Rashba SOI region²¹ and an ac-biased Rashba-type two-dimensional (2D) disorder system²³ or quantum channel.²⁴ It is known that the translational invariance is broken in the channel direction due to a spatially localized time-dependent potential, thus allowing us to explore coherent resonant inelastic scattering and time-modulated quasibound state features.²⁵

In addition to the Rashba SOI,¹⁹ which is caused by the structure inversion asymmetry of the confining potential of the 2D trapping well, there is also a Dresselhaus effect²⁶ caused by the bulk inversion asymmetry²⁷ (BIA) and the

interface inversion asymmetry (IIA).²⁸ The contributions associated with BIA and IIA are phenomenologically inseparable. The Rashba effect is usually dominant, but the Dresselhaus effect could be also observable.²⁹ In this article, we consider a narrow channel formed in a high-mobility electronic quantum well by applying negative bias on the front split gates. When a finger gate is deposited above the split gate separated by an insulating layer, a local time varying Rashba coupling parameter $\alpha(\mathbf{r}, t)$ can be induced by ac-biasing the finger gate.^{21,24} We shall explore how the interplay among the static Rashba, the static Dresselhaus, and the dynamical Rashba SOI effects influences the efficiency of spin current generation in the absence of source-drain bias. The considered dynamical system for spin pumping is depicted in Fig. 1.

The electron transport in a narrow channel in the presence of SOI can be described by the dimensionless Hamiltonian,²⁵

$$\mathcal{H}_0 = k^2 + \mathcal{H}_{\text{SO}}^0 + V_c(y), \quad (1)$$

where the first term $k^2 = k_x^2 + k_y^2$ denotes the kinetic energy and the third term $V_c(y) = \omega_y^2 y^2$ is a potential that confines the electron in the y direction. For a narrow quantum well along the $[0, 0, 1]$ crystallographic direction, the unperturbed SOI term $\mathcal{H}_{\text{SO}}^0$ involving Rashba and Dresselhaus interaction effects can be described in terms of k -linear form,

$$\mathcal{H}_{\text{SO}}^0 = \mathcal{H}_{\text{R}}^0 + \mathcal{H}_{\text{D}}^0 = \alpha_0(\sigma_x k_y - \sigma_y k_x) + \beta_0(\sigma_x k_x - \sigma_y k_y), \quad (2)$$

where σ_i ($i = \{x, y, z\}$) are the Pauli matrices and $\mathbf{k} = (k_x, k_y)$ is the 2D electron wave vector. The unperturbed Rashba coupling strength α_0 is proportional to the electric field along \mathbf{z} direction perpendicular to the 2D electron gas. Moreover, the Dresselhaus coupling strength β_0 is determined by the semiconductor material and the geometry of the sample.

^{a)}Electronic mail: cstang@nuu.edu.tw

^{b)}Electronic mail: whkuan@phys.cts.nthu.edu.tw

^{c)}Electronic mail: wen105@rsphysse.anu.edu.au

^{d)}Electronic mail: yiachang@gate.sinica.edu.tw

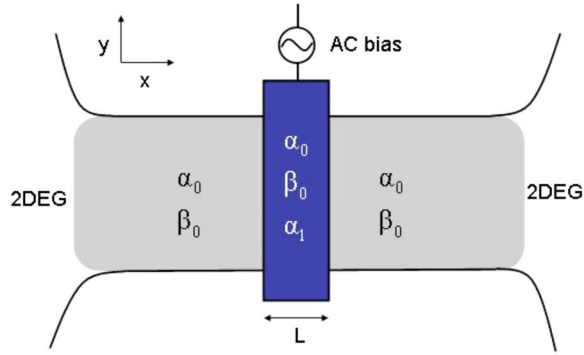


FIG. 1. Schematic illustration of the quantum wire with Rashba and Dresselhaus spin-orbit interaction influenced by an ac-biased finger gate (with length L) across the wire.

For a narrow wire,³⁰ the spin-orbit coupling contributions can be simplified as $\mathcal{H}_{\text{SO}}^0 \approx -\alpha_0 \sigma_y k_x + \beta_0 \sigma_x k_x$. The right-going (left-going) eigenfunctions of the unperturbed Hamiltonian in the subband n are given by

$$\psi_{nk\sigma}^{R(L)}(\mathbf{r}) = \exp[ik_{n\sigma}^{R(L)}(\mu)x] \varphi_n(y) \chi_\sigma, \quad (3)$$

where $\sigma = \pm$ labels the two spin branches, χ_σ is the spinor of branch σ with two components given by $e^{i\theta/2}/\sqrt{2}$, and $\sigma e^{-i\theta/2}/\sqrt{2}$ with $\theta = \arctan(\alpha_0/\beta_0)$. In addition, the wave vectors are defined by $k_{n\sigma}^R(\mu) = \sqrt{\mu - \varepsilon_n - \sigma\gamma_0}/2$ and $k_{n\sigma}^L(\mu) = -\sqrt{\mu - \varepsilon_n - \sigma\gamma_0}/2$, where μ is the chemical potential, $\gamma_0 = (\alpha_0^2 + \beta_0^2)^{1/2}$, and ε_n is the subband threshold, which is shifted from the bare subband bottom $\varepsilon_n^0 = (2n+1)\omega_y$ by $-\gamma_0^2/4$. The total Hamiltonian $\mathcal{H} = \mathcal{H}_0 + \mathcal{H}_{\text{SO}}(t)$ contains a dynamical term, induced by the ac-biased finger gate, which can be written in the form

$$\mathcal{H}_{\text{SO}}(t) = -\frac{\alpha_1}{2} \sigma_y \{k_z, \theta(L/2 - |x|)\} \cos \omega t, \quad (4)$$

where $\theta(x)$ is the step function and $\{, \}$ stands for anticommutator.

Below, we assume that the Dresselhaus SOI is weak and neglect the spin-flip mechanism. The scattering wave function of the conduction electron incident from the left reservoir in the spin state σ can be obtained of the form $\Psi_\sigma(\mathbf{r}, t) = \sum_n \psi_{n\sigma}(x, t) \varphi_n(y) \chi_\sigma$. In the region $x < -L/2$, the time-dependent wave function along the channel direction is given by

$$\psi_{n\sigma}(x, t) = e^{ik_{n\sigma}^R(\mu)x} e^{-i\mu t} + \sum_m r_{n\sigma}^m e^{ik_{n\sigma}^L(\mu_m)x} e^{-i\mu_m t}, \quad (5)$$

where $\mu_m \equiv \mu + m\omega$ and $r_{n\sigma}^m$ denotes the reflection coefficient of the conduction electron in the subband n and photon sideband m . In the region $x > L/2$, the wave function is simply of the form

$$\psi_{n\sigma}(x, t) = \sum_m t_{n\sigma}^m e^{ik_{n\sigma}^R(\mu_m)x} e^{-i\mu_m t}, \quad (6)$$

where $t_{n\sigma}^m$ indicates the corresponding transmission coefficient. The longitudinal wave function in the time-modulated region $|x| < L/2$ is given by²⁵

$$\begin{aligned} \psi_{n\sigma}(x, t) = \sum_{m'p} \left\{ A_{n\sigma}^{m'} e^{ik_{n\sigma}^R(\mu_m)x} J_p \left(k_{n\sigma}^R(\mu_{m'}) \frac{\alpha_1}{\omega} \right) \right. \\ \left. + B_{n\sigma}^{m'} e^{ik_{n\sigma}^L(\mu_m)x} J_p \left(k_{n\sigma}^L(\mu_{m'}) \frac{\alpha_1}{\omega} \right) \right\} \\ \times \exp[-i\mu_{m'+p} t] \sigma_p, \end{aligned} \quad (7)$$

where $\sigma_p = 1$ if p is even and $\sigma_p = -\sigma_y$ if p is odd. Performing the time-dependent mode matching at $x = \pm L/2$,²⁴ one can obtain the reflection and transmission coefficients, $r_{n\sigma}^m$ and $t_{n\sigma}^m$, at the edges of the time-modulated region. Similarly, it is easy to obtain $\tilde{r}_{n\sigma}^m$ and $\tilde{t}_{n\sigma}^m$ for the conduction electrons incident from the right reservoir.

Summing over all possible scattered propagating modes from both reservoirs, the net right-going dc spin current can be expressed as $I_S = I^\uparrow - I^\downarrow$, where

$$I^\sigma = \frac{e}{h} \int dE f(E) [T_{RL}^\sigma + T_{LR}^{\bar{\sigma}}], \quad (8)$$

with $f(E)$ being the Fermi function in the reservoirs. In addition, $T_{RL}^\sigma = \sum_n \sum_m |t_{n\sigma}^m|^2 v_n^m / v_n^0$ and $T_{LR}^{\bar{\sigma}} = \sum_n \sum_m |\tilde{t}_{n\sigma}^m|^2 v_n^m / v_n^0$, where $v_n^m \equiv (\mu_m - \varepsilon_n)^{1/2}$. The spin current conservation is maintained due to the suppression of spin-flip subband mixing. Since a symmetric narrow channel configuration gives $T_{LR}^\sigma = T_{RL}^{\bar{\sigma}}$, the net charge current $I_Q = I^\uparrow + I^\downarrow$ is identically zero, and a pure nonequilibrium spin current is generated. It turns out that the two charge currents for both spin types have identical values but opposite directions. Therefore, the generated pure spin current implies the fully polarized charge current.³¹

The calculations presented below are carried out under the assumption that the electron effective mass $m^* = 0.036m_0$, which is appropriate to the InGaAs–InAlAs interface. The typical electron density $n_e \sim 10^{12} \text{ cm}^{-2}$ and $\hbar\alpha_0 \sim 10^{-11} \text{ eV m}$.¹⁸ We select $\omega_y = 0.035$ such that the subband level spacing, $\Delta\varepsilon = 2\omega_y$, is 4.13 meV. Accordingly, the length unit $L^* = 4.0 \text{ nm}$, the energy unit $E^* = 59 \text{ meV}$, and the spin-orbit coupling parameters are in units of $v_F^*/2 = 1.8 \times 10^5 \text{ m/s}$.

In Fig. 2, we demonstrate how the Dresselhaus spin-orbit coupling strength influences the dc spin current generated by the ac-biased front gate with driving region $L = 120 \text{ nm}$. The other parameters are static Rashba parameter $\hbar\alpha_0 = 1.5 \times 10^{-11} \text{ eV m}$, $\alpha_1 = 0.38\alpha_0$, and $\hbar\omega = 0.2 \text{ meV}$. In Fig. 2(a), the sharp dip structure at $K \approx \omega$ is the one-photon quasibound state feature.²⁵ For electron energies at $1 < K/\omega < 2$, we see clearly $T_{RL}^\uparrow < T_{RL}^\downarrow$ leading to positive spin current. The change in sign in the transmission difference $\Delta T_{RL} = T_{RL}^\uparrow - T_{RL}^\downarrow$ comes across the dip structures, that is, $\Delta T_{RL}(K = \omega^-) > 0$, while $\Delta T_{RL}(K = \omega^+) < 0$. Consequently, for electrons with incident energy $K/\omega \approx 1$, the spin current peak is generated within the order of 1 nA, as is shown in Fig. 2(b).

For the cases of zero and weak Dresselhaus SOI such as $\beta_0 = 0.0$ and 0.02, the electrons with energy $K/\omega \approx 2$ exhibit small dip structures which is associated with two-photon quasibound state feature. Since at $K/\omega \approx 2$ the current trans-

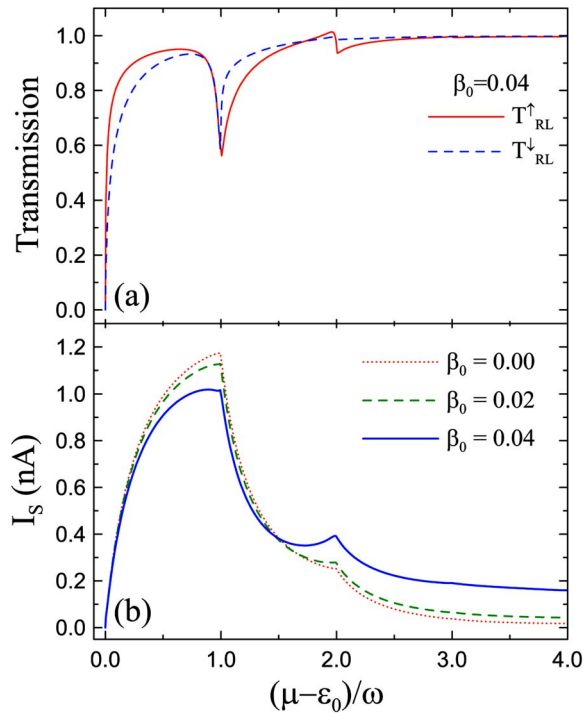


FIG. 2. (a) Spin-resolved current transmission T_{RL}^{\uparrow} (solid red) and T_{RL}^{\downarrow} (dashed blue) as a function of electron energy in units of driving frequency. (b) Generated dc spin current for the cases of $\beta_0=0.0$ (dotted red), 0.02 (dashed green), and 0.04 (solid blue). $L/L^*=30$, $\alpha_0=0.13$, $\alpha_1=0.05$, and $\omega=0.05\Delta\varepsilon$.

mission T_{RL}^{\uparrow} of spin- \uparrow electron is still less than T_{RL}^{\downarrow} of the spin- \downarrow electron, there is no significant contribution to the generation of dc spin current. In Fig. 2(a), we show the current transmission for the case of strong Dresselhaus coupling $\beta_0=0.04$. The right-going spin- \uparrow electron manifests Fano-type peak-and-dip line shape in transmission at $K \approx 2\omega$, which is associated with the two-photon quasibound state feature. This Fano-type feature enhances T_{RL}^{\uparrow} to be greater than T_{RL}^{\downarrow} . Consequently, the pumped dc spin current is thus significantly enhanced. We would like to mention in passing that the Fano spin filtering effects may be realized in an open quantum dot³² or a stub waveguide system.³³

In the absence of Dresselhaus effect, the electron in the low kinetic energy regime may be multiple scattered by the transverse confining potential, such that the spin orientation is mainly along the wire direction. The Dresselhaus effect plays a role to rotate the spin direction toward the y direction. Consequently, the net spin current is thus enhanced. However, the spin direction of an electron in the high kinetic energy regime is mainly perpendicular to the wire direction, the Dresselhaus effect thus plays a role to enhance the spin current generation.

Figure 3 shows the spin-resolved transmission with dynamical Rashba coefficient $\alpha_1=0.05$ and the generated dc spin current for cases of $\alpha_1=0.03, 0.04$, and 0.05 . The other parameters are ac-driven region $L=200$ nm, Rashba strength $\hbar\alpha_0=1.5 \times 10^{-11}$ eV m, Dresselhaus strength $\beta_0=0.23\alpha_0$, and driving frequency $f=\omega/2\pi=50$ GHz. There are com-

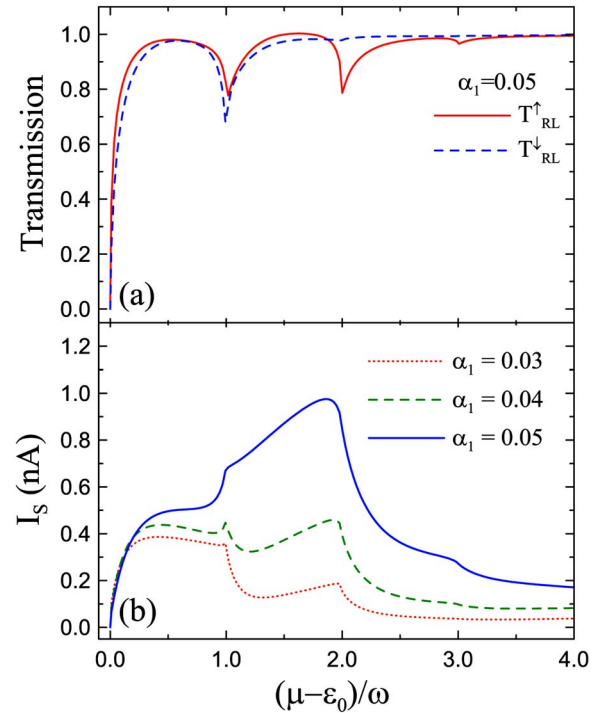


FIG. 3. (a) Spin-resolved current transmission T_{RL}^{\uparrow} (solid red) and T_{RL}^{\downarrow} (dashed blue) as a function of electron energy in units of driving frequency. (b) Generated dc spin current for the cases of $\alpha_1=0.03$ (dotted red), 0.04 (dashed green), and 0.05 (solid blue). $L/L^*=50$, $\alpha_0=0.13$, $\beta_0=0.03$, and $\omega=0.05\Delta\varepsilon$.

mon transport features for the three different dynamical coupling strengths. The overlap of I_S curves for the incident electron energies $K/\omega \leq 0.2$ implies that the transport properties are insensitive to the driving strength in the very low kinetic energy regime. The similar plateau features in I_S at $K/\omega < 1.0$ are caused by the competition of the current transmission of spin- \uparrow and spin- \downarrow electrons.

At incident electron energy $(\mu-\varepsilon_0)/\omega \approx 1.0$, there are kink structure in I_S for $\alpha_1=0.03$, peak structure for $\alpha_1=0.04$, and shoulder structure for $\alpha_1=0.05$. For the case of $\alpha_1=0.03$, the current transmissions of the two spin states are almost the same at $K=\omega^-$, exhibiting plateau feature, while the transmission of the spin- \uparrow electron is smaller than the spin- \downarrow at $K=\omega^+$, exhibiting strong drop feature in I_S . For the case of $\alpha_1=0.04$, the crossover in the transmission for two spin states leads to the peak structure at $K \approx \omega$. However, for the case of $\alpha_1=0.05$, we see that T_{RL}^{\uparrow} is greater than T_{RL}^{\downarrow} until the crossover at $K/\omega=1.87$ leading to the shoulder behavior in I_S . This feature in combination with the broad dip structure, associated with electrons emitting two photons to the subband threshold forming a quasibound state, results in the broad spin current peak $I_S=0.98$ nA at $K/\omega=1.87$. Small hill in I_S at $K/\omega \approx 3.0$ is barely recognized. At $K/\omega=4.0$, the spin currents are nearly saturated to $I_S=0.04, 0.08$, and 0.17 nA for $\alpha_1=0.03, 0.04$, and 0.05 , respectively.

In this article, we have investigated nonadiabatically how the dc spin current is generated under the mechanism of SOI using a dynamical all electrical control on a split-gate-

confined narrow channel. We have demonstrated nontrivial features concerning the spin current generation mechanism caused by different strength of Dresselhaus spin-orbit coupling. These results provide a robust manner of generating spin current without accompanying charge current.

The spin current generating features have been demonstrated and illustrated in detail. It has been found that the Dresselhaus spin-orbit coupling intends to suppress the efficiency of spin current generation in the low kinetic energy regime, while the Dresselhaus effect can enhance the pumped spin current in the high kinetic energy regime. Unlike the parametric quantum pumping, in which two pumping potentials with a phase difference are needed,⁹ Our proposed spin current generating device is achievable using a single ac-biased gate and should be achievable within recent fabrication capability.

The authors acknowledge the financial support by the National Science Council and the Academia Sinica in Taiwan. C.S.T. is grateful to inspiring discussions with L. Y. Wang and C. S. Chu, and the computational facility supported by the National Center for High-Performance Computing of Taiwan.

¹*Semiconductor Spintronics and Quantum Computation*, edited by D. D. Awschalom, N. Samarth, and D. Loss (Springer-Verlag, Berlin, 2002).

²S. A. Wolf, D. D. Awschalom, R. A. Buhrman, J. M. Daughton, S. von Molnár, L. Roukes, A. Y. Chtchelkanova, and D. M. Treger, *Science* **294**, 1488 (2001).

³S. Murakami, N. Nagaosa, and S. C. Zhang, *Science* **301**, 1348 (2003).

⁴Y. K. Kato, R. C. Myers, A. C. Gossard, and D. D. Awschalom, *Science* **306**, 1910 (2004).

⁵J. Sinova, D. Culcer, Q. Niu, N. A. Sinitsyn, T. Jungwirth, and A. H. MacDonald, *Phys. Rev. Lett.* **92**, 126603 (2004); J. Wunderlich, B. Kaestner, J. Sinova, and T. Jungwirth, *ibid.* **94**, 047204 (2005).

⁶B. A. Bernevig and S. C. Zhang, *Phys. Rev. Lett.* **96**, 106802 (2006).

⁷S. O. Valenzuela and M. Timkham, *Nature (London)* **442**, 176 (2006).

⁸V. Sih, W. H. Lau, R. C. Myers, V. R. Horowitz, A. C. Gossard, and D. D.

Awschalom, *Phys. Rev. Lett.* **97**, 096605 (2006); N. P. Stern, S. Ghosh, G. Xiang, M. Zhu, N. Samarth, D. D. Awschalom, *ibid.* **97**, 126603 (2006).

⁹E. R. Mucciolo, C. Chamon, and C. M. Marcus, *Phys. Rev. Lett.* **89**, 146802 (2002); S. K. Watson, R. M. Potok, C. M. Marcus, and V. Umansky, *ibid.* **91**, 258301 (2003).

¹⁰A. Brataas, Y. Tserkovnyak, G. E. W. Bauer, and B. I. Halperin, *Phys. Rev. B* **66**, 060404 (2002).

¹¹P. Zhang, Q. K. Xue, and X. C. Xie, *Phys. Rev. Lett.* **91**, 196602 (2003).

¹²B. G. Wang, J. Wang, and H. Guo, *Phys. Rev. B* **67**, 092408 (2003).

¹³Q. F. Sun, H. Guo, and J. Wang, *Phys. Rev. Lett.* **90**, 258301 (2003).

¹⁴W. Zeng, J. L. Wu, B. G. Wang, J. Wang, Q. F. Sun, and H. Guo, *Phys. Rev. B* **68**, 113306 (2003).

¹⁵R. D. R. Bhat and J. E. Sipe, *Phys. Rev. Lett.* **85**, 5432 (2000).

¹⁶J. Hubner, W. W. Ruhle, M. Klude, D. Hommel, R. D. R. Bhat, J. E. Sipe, and H. M. van Driel, *Phys. Rev. Lett.* **90**, 216601 (2003).

¹⁷M. J. Stevens, A. L. Smirl, R. D. R. Bhat, A. Najmaie, J. E. Sipe, and H. M. van Driel, *Phys. Rev. Lett.* **90**, 136603 (2003).

¹⁸J. Nitta, T. Akazaki, H. Takayanagi, and T. Enoki, *Phys. Rev. Lett.* **78**, 1335 (1997); D. Grundler, *ibid.* **84**, 6074 (2000).

¹⁹E. I. Rashba, *Sov. Phys. Solid State* **2**, 1109 (1960); Y. A. Bychkov and E. I. Rashba, *J. Phys. C* **17**, 6039 (1984).

²⁰P. Sharma and P. W. Brouwer, *Phys. Rev. Lett.* **91**, 166801 (2003).

²¹M. Governale, F. Taddei, and R. Fazio, *Phys. Rev. B* **68**, 155324 (2003).

²²A. G. Mal'shukov, C. S. Tang, C. S. Chu, and K. A. Chao, *Phys. Rev. B* **68**, 233307 (2003).

²³C. S. Tang, A. G. Mal'shukov, and K. A. Chao, *Phys. Rev. B* **71**, 195314 (2005); For a brief review, see C. S. Tang, *Int. J. Mod. Phys. A* **20**, 869 (2006).

²⁴L. Y. Wang, C. S. Tang, and C. S. Chu, *Phys. Rev. B* **73**, 085304 (2006).

²⁵C. S. Tang and C. S. Chu, *Phys. Rev. B* **53**, 4838 (1996); **60**, 1830 (1999); C. S. Tang, Y. H. Tan, and C. S. Chu, *ibid.* **67**, 205324 (2003).

²⁶G. Dresselhaus, *Phys. Rev.* **100**, 580 (1955).

²⁷M. I. D'yakonov, and V. Yu. Kachorovskii, *Fiz. Tekh. Poluprovodn. (S.-Peterburg)* **20**, 178 (1986); [*Sov. Phys. Semicond.* **20**, 110 (1986)].

²⁸L. Vervoort and P. Voisin, *Phys. Rev. B* **56**, 012744 (1997).

²⁹S. D. Ganichev, V. V. Bel'kov, L. E. Golub, E. L. Ivchenko, P. Schneider, S. Giglberger, J. Eroms, J. DeBoeck, G. Borghs, W. Wegscheider, D. Weiss, and W. Prettl, *Phys. Rev. Lett.* **92**, 256601 (2004).

³⁰R. G. Pereira and E. Miranda, *Phys. Rev. B* **71**, 085318 (2005).

³¹J. Wang, K. S. Chan, and D. Y. Xing, *Phys. Rev. B* **72**, 115311 (2005).

³²J.-F. Song, Y. Ochiai, and J. P. Bird, *Appl. Phys. Lett.* **82**, 4561 (2003).

³³Feng Zhai and H. Q. Xu, *Phys. Rev. B* **76**, 035306 (2007).